PULSED FIELD OF A MAGNETISING COIL WOUND WITH A SOLID CONDUCTOR OF RECTANGULAR CROSS-SECTION

By:

PATRICK GIBSON.

POSTGRADUATE STUDENT U.C.T. ELECTRICAL ENGINEERING DEPARTMENT

Supervisors:

DR R.E. NEUBAUER.

CHIEF TECHNICAL OFFICER MR J. HESSELINK.

REPORT SUBMITTED FOR DEGREE OF MASTERS OF SCIENCE IN ENGINEERING 30 APRIL 1990

ACKNOWLEDGEMENTS.

I would like to thank my supervisor Dr R.E. Neubauer, for the countless interesting hours he has devoted to guiding me through the wonders of Electromagnetic theory. Also much thanks must go to Chief Technical Officer Mr. J. Hesselink for the enthusiastic, inspirational and much appreciated technical support he contributed to this project.

SYNOPSIS.

This report describes a mathematical approach to solving the pulsed magnetic field for an N-turned magnetising coil. This coil is assumed to be made from a copper conductor with rectangular cross-sectional area. The algorithm accounts for each turns physical dimensions and spatial coordinates with respect to other turns, by simulating each winding with a model helical turn. A boundary matching method is used to determine the current density distribution in the 2D plane of the coil conductor and the changed impedance due to "skin-effect". By assuming this distribution and changed impedance applies for the N-turned coil volume, the effects of eddy current losses are approximated inside the coil.

Results of comparing field calculations with several analytical field solutions for static fields, and by measurements for pulsed fields, confirms the accurracy of the field algorithm in approximating a real coil field to within 10 % error. This algorithm can thus be used to aid the design of coils for generation of saturation fields for magnetisation of different ferromagnetic materials.

TABLE OF CONTENTS

1 INTRODUCTION

Although South Africa has an abundance of natural elements, magnetisation and manufacture of ferromagnetic materials has received minimal research. Permanent magnets have to be imported by companies when needed for commercial applications. To introduce this technology to South Africa, a project was undertaken in the Electrical Engineering Department of U.C.T., for the design and construction of a prototype magnetising unit.

Advanced material technology has produced high quality permanent magnets eg Rare Earth types. As a result, the applications for these quality magnets in systems and devices has become numerous. Countless industrial journals, eg. [1] [2] and literature [3] [4] are available about magnets and the process of magnetisation. These texts usually describe general technical information, and may supply data tables for different materials. Seldom is much attention given to the magnetising unit itself. While the units circuitry in general is simple, the magnetising coil may be the most complex and expensive component. Numerous coil configurations are available, which in some designs may include water-cooling, for repeated use after short intervals.

The prototype magnetiser constructed at U.C.T. was to be used for research and experimental applications only. To keep costs minimal, the magnetising coil was wound using copper wire having a rectangular cross sectional area. For efficient magnetisation of a material, it is necessary to have a field that will cause saturation inside the probe. It is impossible to predict without an aid, the field inside different coil configurations. This is because of the fields dependency on conductor dimensions and spatial orientation of the coil turns.

To help design coils for generation of different field strengths, a theoretical model has been developed. This model approximates the pulsed field inside coils of different configurations. The algorithm is unique in that it accounts for the effect on field of the conductor's physical dimensions. Also the effect of each turns spatial orientation with respect to the other turns and eddy losses is considered. The algorithm can be used to predict the number of turns needed for a specific field intensity and as an aid in determining how the coil should best be wound.This report describes the

mathematical development of the algorithm used to approximate the field inside different coil designs.

Because the project was unsponsored, progress was often delayed by financial limitations. Alternative low-cost options had to be found for several technical obstacles. As an example, a suitable Gaussmeter for field measurements had to be designed and constructed. Difficulties were also experienced in obtaining a suitable switch for "clean high voltage switching". This led to a delay of several months, while alternatives were investigated.

REFERENCES

[1] Dr Steingrover GMBH,"How to Magnetise, Demagnetise and calibrate Permanent Magnets",Magnet-Physic (MPS),1988 Edition,Koln West Germany.

[2] Magnetfabrik Schramberg Brochure,Schramberg West Germany.

[3] W. Wright and M. McCraig, Permanent Magnets, Engineering Design Guide No 20, Published for the Design Council, the British Standards Institution and the Council of Engineering Institutions by Oxford University Press, U.K. 1977.

[4] William Taussig Scott, The Physics of Electricity and Magnetism, New York, John Wiley and Sons, 2nd Edition,1966, Chapter 8.

2.PROCESS OF MAGNETISATION.

Several electrical methods are used to magnetise ferromagnetic materials.[5] In general, the magnet is subject to a large unidirectional field which must saturate the material, if maximum magnetic conditions such as the largest BH energy product are to be realised. Saturation for most magnets occurs in fields of less than 10 Tesla [5]. The most economical and practical way of obtaining fields below 10 Tesla, is by generating pulsed fields inside wire-wound coils.[7]

The circuit shown in Fig. 2.1 is the prototype magnetiser used in this project, to generate current pulses of large magnitude and time duration through a magnetising coil. A large pulsed magnetic field is generated for the coil, when a large current pulse flows. Typical pulse time durations of 10 milli-seconds or greater are possible with this arrangement. Initially assuming eddy current losses are negliable, the coil is approximated by an RL series network, where resistive and inductive values R and L are measured at DC.

r - charging resistor

L - Inductance of coil

R - Coil resistance

T - Step up Transformer

Hv - High voltage

[region of Kilovolts]

D1 - Freewheel diode

C - Capacitor bank

S2 - High voltage switch eg.

- thyristors,vacuum switches

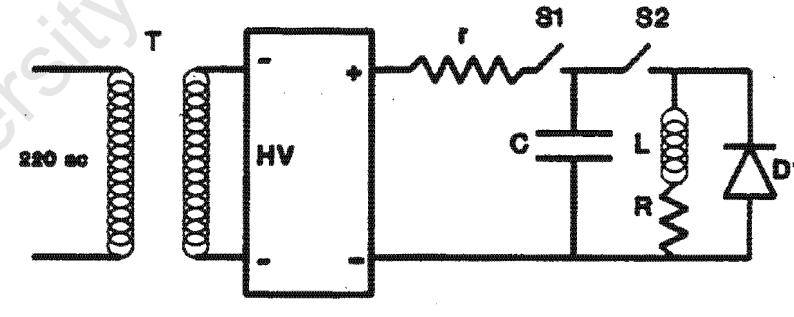

Figure 2.1 Magnetising circuit that generates a large magnetic pulse of long time duration for magnetisation of a ferromagnetic material.

The circuit operates on a stored energy principle.The capacitor bank is charged (closing S1) via a transformer and a rectifier for a period of seconds. Once charged to the required voltage, S1 is opened and S2 closed. This discharges the stored energy into the coil. Typical transient current and voltage waveforms for the coil are shown in Figs. 2.2a and 2.2b.

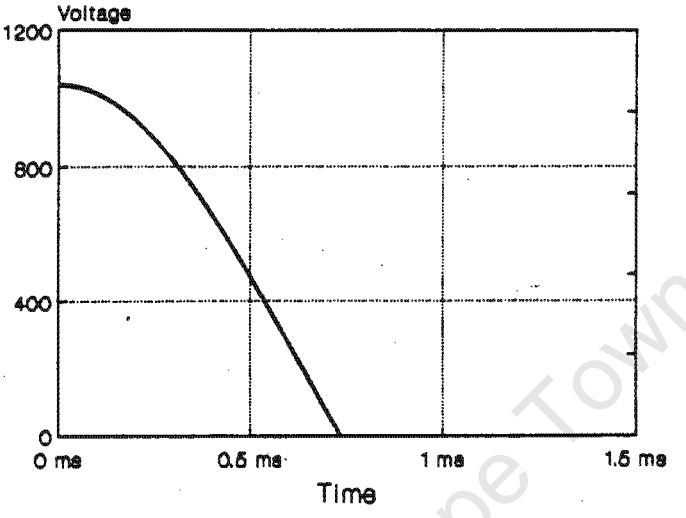

Figure 2.2a Typical transient voltage across the coil
V = 1000 volts, C = 960 microFarads, L = 0.2 milliHenries,R = 0.085 ohms

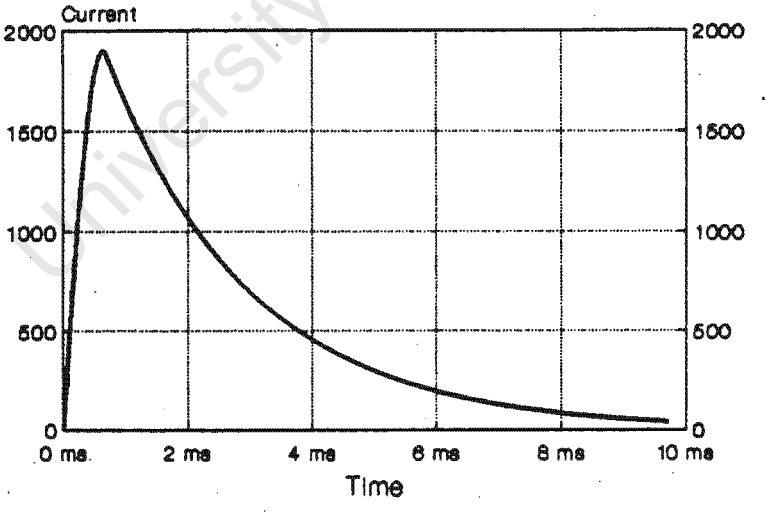

Figure 2.2b Typical transient current pulse through the coil
V = 1000 volts, C = 960 microFarads, L = 0.2 milliHenries,R = 0.085 ohms

Upon switching the capacitor bank across the coil, the voltage falls to zero while the current rises to a maximum. If it were not for the free-wheeling diode, the current would oscillate*. The function of the diode is to clamp the capacitor voltage to zero and let the current decay exponentially, providing an increased pulse length.

The current pulse is described separately by two equations before and after the diode conducts. These are:

$$i\left(t < t_{peak}\right) = \frac{V}{Lw} \sin(wt) \exp\left[-\frac{t}{\tau}\right] \qquad 2.1$$

$$i\left(t > t_{peak}\right) = I_{peak} \exp\left[-\left(t - t_{peak}\right)\frac{R}{L}\right] \qquad 2.2$$

$$\tau = 2\frac{L}{R} \qquad w = \sqrt{\frac{1}{LC} - \frac{1}{\tau^2}} \qquad t_{peak} = \frac{arctan(w\tau)}{w}$$

with: $$I_{peak} = \frac{V}{Lw}\sin[arctan(wt)] \frac{\exp\left[-arctan(w\tau)\right]}{w\tau}$$

t - Time

t_{peak} - Time at which the freewheel diode starts conduction.

V - Capacitor bank voltage

L - Dc coil inductance

R - Dc coil resistance

C - Capacitor bank

* *If the current was allowed to oscillate, the magnet would be demagnetised.*

The critical resistance Rcrit of the circuit is expressed as:

$$R_{crit} = 2\sqrt{\frac{L}{C}}$$

From experience typical magnetisers were found to have critical resistances of 1 ohm. It is essential for the following reasons to have the coil resistance well below Rcrit:

i) Increased coil resistance means less peak current being generated for a given magnetiser setup ie. the circuit becomes damped and less field is generated.

ii) The bandwidth of the current pulses is inversely proportional to the pulse time duration. Thus eddy current losses become greater with decrease in the time duration of the pulse (ie increased R). This results in a weaker field being generated inside the coil and less peneration depth inside the ferromagnetic material. Especially materials which are conductive.

The effects of R,L,C on the magnitude of the current pulse is illustrated graphically in Figs. 2.3 a-c.

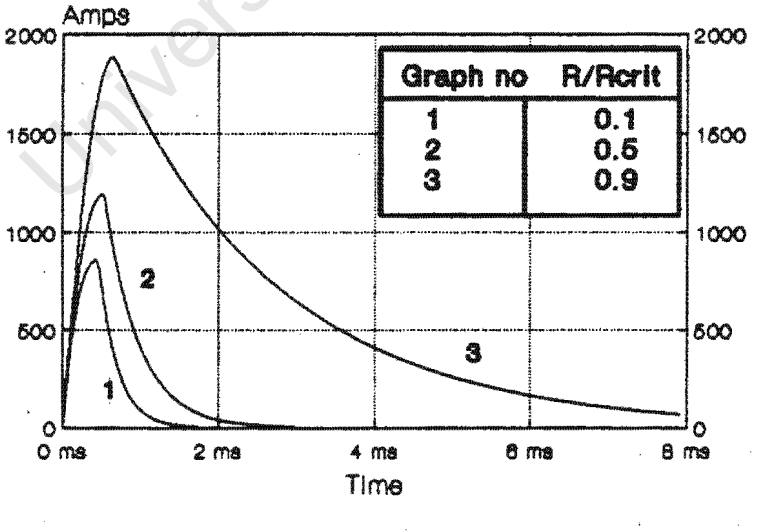

Figure 2.3a Effect of coil resistance on current pulse magnitude and duration.
V = 1000 volts, C = 960 microFarads, L = 0.2 milliHenries

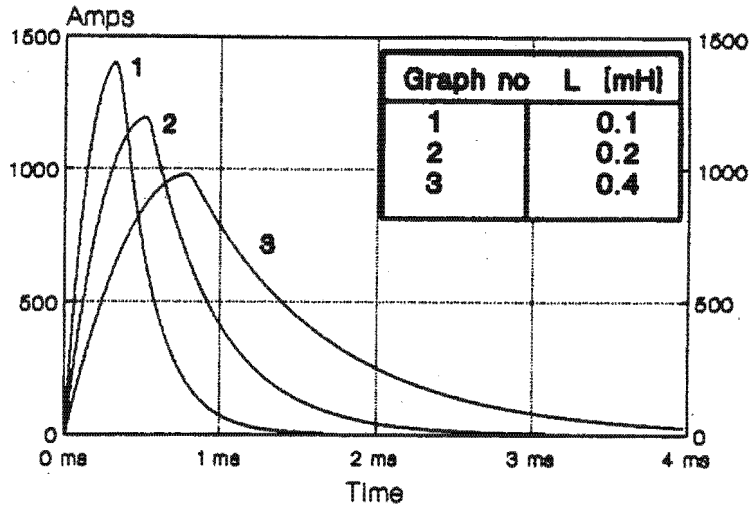

Figure 2.3b Effect of inductanceFigure 2.3b Effect of inducance on current pulse magnitude and duration
V = 1000 volts, C = 960 microFarads, R = 0.045 ohms

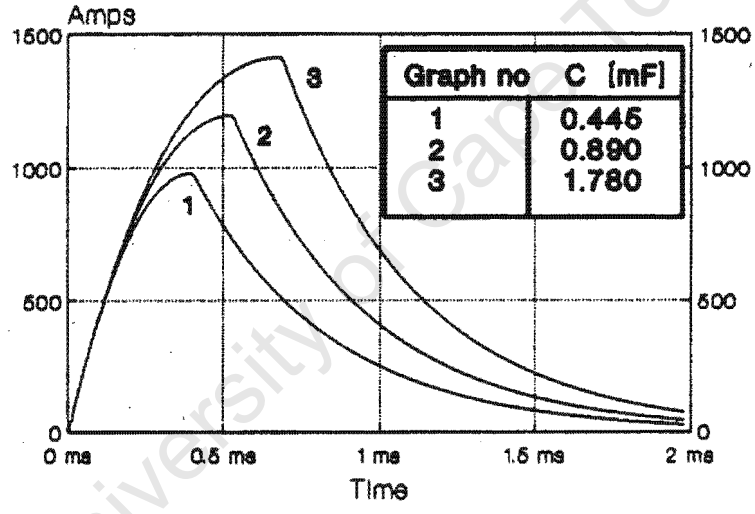

Figure 2.3c Effect of capacitance on current pulse magnitude and duration
V = 1000 volts, R = 0.045 ohms, L = 0.2 milliHenries

REFERENCES.

[5] Magnetics, RFC Industries Inc, Boonton,New Jersey,U.S.A.

[6] see [5]

[7] Fritz Herlach,"The Technology of Pulsed High Magnets", IEEE Trans. of Magn., Vol Mag-24, No 2, March 1988, P1049-1051.

3. ANALYSIS OF AN N-TURNED COIL.

3.1 Coil Model

The physical dimensions of a coil are dependent upon conductor size and method of coil construction. Each turn has it's own unique spatial dimension and orientation around the core center. Successive turns of similar diameter, usually spiral vertically up and down the coil core forming a helix. The coil may also have several lateral helix layers of increasing diameter. To determine accurately the field for a given current strength all the above should be considered.

The fundamental "building block" for the algorithm is a model of a single helical coil turn (Fig 3.1). This turn is assumed made from copper wire having a rectangular cross-sectional area. A coil of many turns is approximated by assuming it as the assemble of numerous of these model turns. As an example consider the following: If m anti-clockwise orientated turns having equal radius are linked together, a right-handed helix of m turns is realised. Similarly m clockwise orientated turns joined together form a left-handed helix. By encasing alternatively, right-handed and left-handed helixes of increasing diameter around each other, an nxm simulation coil is developed. Using alternative left and right handed helixes accounts for current flow up and down the coil. This model of an nxm-turned coil approximates a real wire-wound coil and can be used for field analysis. The total field at any spatial coordinate is by superposition, the summation of field contributions from each of the nxm turns.A disadvantage of the model is the discontinuity that exists at the junction between successive overlapping helixes which has not been taken into account in this model.

3.2 Mathematical Analysis

The time dependent magnetic field for the 3D current carrying helical arrangement of Fig. 3.1 is solved using Biot-Savart's method. In a medium of permeability μ_0, the field intensity $\vec{H}(\vec{r}_P)$ is given by the following equation:[8]

$$\vec{H}(\vec{r}_P,t) = \frac{1}{4\pi}\vec{\nabla}\times\int\int\int_{V'}\frac{\vec{J}(\vec{r}_Q,t)}{\vec{r}}dV' \qquad 3.1$$

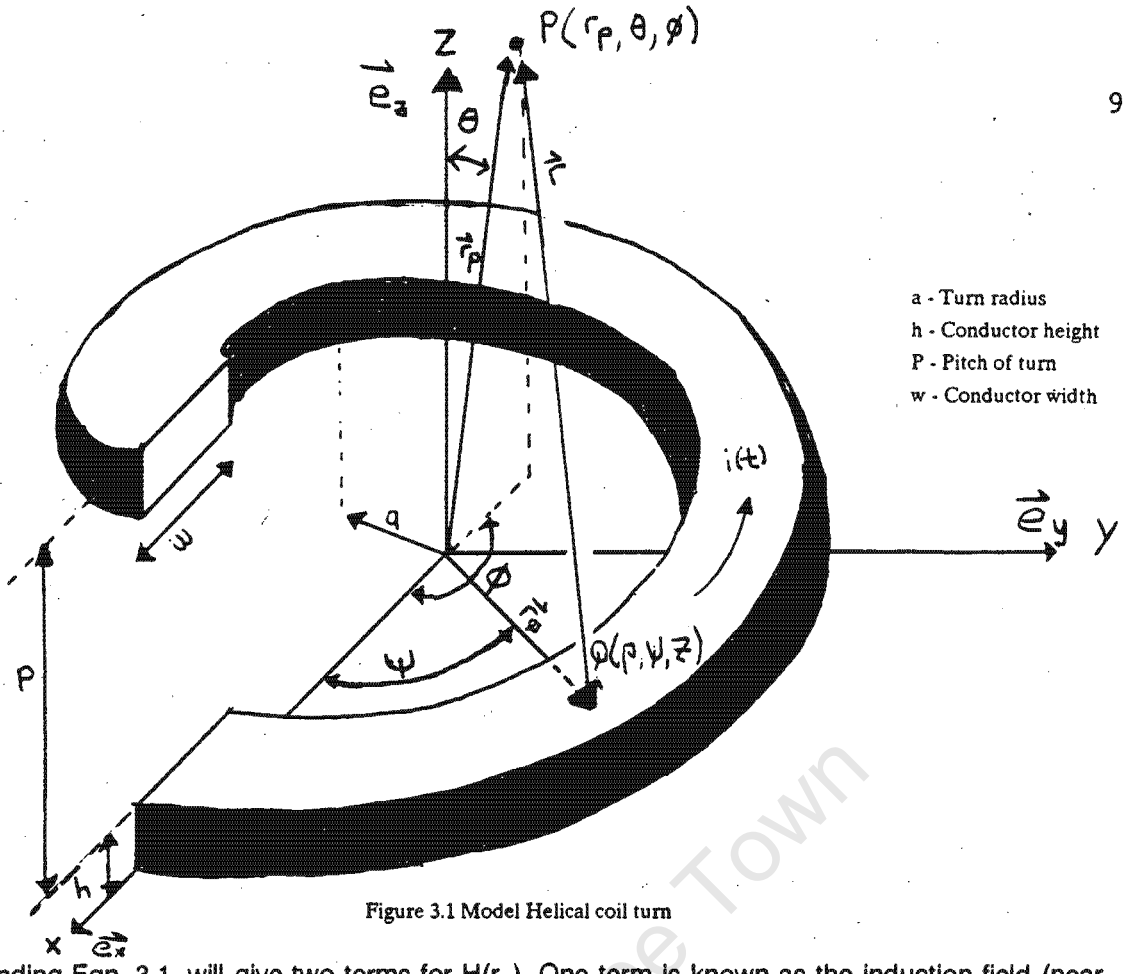

Figure 3.1 Model Helical coil turn

Expanding Eqn. 3.1, will give two terms for $H(r_P)$. One term is known as the induction field (near field) while the other term is the radiation field (far field). The magnetising pulse has a bandwidth in the lower khz region and thus the radiation term can be neglected. The induction field $H(r_P)$ is thus given by:

$$\vec{H}(\vec{r}_P, t) = \frac{1}{4\pi} \int\int\int_{V'} \frac{\vec{J}(\vec{r}_Q, t) \times \vec{r}}{|\vec{r}|^3} dV' \qquad 3.2$$

with:

V' – helical coil turn volume $\quad dV' = \rho \, d\rho \, d\psi \, dz$

$\vec{J}(\vec{r}_Q, t)$ – time-dependent current density

$\vec{r}_P$ – position vector of field point defined by the spherical coordinate:

$$(r_p, \theta, \phi) \rightarrow r_p \in [0, \infty] \quad \theta \in [0, \pi] \quad \phi \in [0, 2\pi]$$

$\vec{r}_Q$ – position vector of source point defined by the cylindrical coordinate:

$$(\rho, \psi, z) \rightarrow \rho \in [a, a+w] \quad \psi \in [\phi, \phi + 2\pi] \quad z \in [p\psi/2\pi, p\psi/2\pi + h]$$

$\vec{r}$ – distance vector between field point and current source defined by:

$$\vec{r} = \vec{r}_p - \vec{r}_Q$$

Writing the displacement vectors in the XYZ co-ordinate system:

$$\vec{r}_P = r_P \sin\theta \cos\phi\, \vec{e}_x + r_P \sin\theta \sin\phi\, \vec{e}_y + r_P \cos\theta\, \vec{e}_z$$

$$\vec{r}_Q = \rho \cos\psi\, \vec{e}_x + \rho \sin\psi\, \vec{e}_y + z\, \vec{e}_z$$

$$\vec{r} = r_x \vec{e}_x + r_y \vec{e}_y + r_z \vec{e}_z$$

with:

$$r_x = r_P \cos\theta \cos\phi - \rho \cos\psi$$

$$r_y = r_P \sin\theta \sin\phi - \rho \sin\psi$$

$$r_z = r_P \cos\theta - z$$

The current density vector $\vec{J}(\vec{r}_Q,t)$ lies in the azimuthal direction to the conductor's cross-sectional plane. In the XYZ reference $\vec{J}(\vec{r}_Q,t)$ is written as:

$$\vec{J}(\vec{r}_Q,t) = -\sin\psi\, J_h \vec{e}_x + \cos\psi\, J_h \vec{e}_y + J_z \vec{e}_z$$

with:

$$J_h = |\vec{J}(\vec{r}_Q,t)| \cos\gamma \qquad J_z = |\vec{J}(\vec{r}_Q,t)| \sin\gamma$$

The pitch angle γ defined by:

$$\gamma(p,\rho) = arctan\left[\frac{p}{2\pi\rho}\right] \qquad 3.3$$

is the angle between the azimuthal direction and the tangent to the conductor at a given source point. For ease of illustration, the pitch angle is shown for a helical coil having a small cross-sectional area (Fig. 3.2).

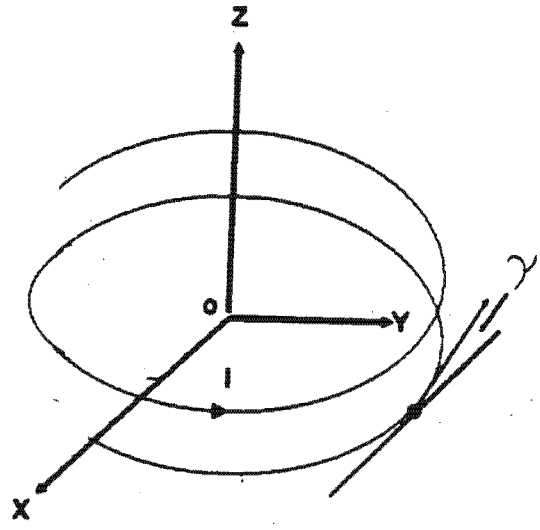

Figure 3.2 Pitch angle τ of a helical coil.

Using Eqn 3.2, the magnetic field intensity $\vec{H}(\vec{r}_p)$ is written into separate vector components as:

$$H_x(\vec{r}_p,t)=\frac{1}{4\pi}\int\int\int_{V'}\frac{r_z J_h\cos\psi - r_y J_z}{|\vec{r}|^3}dV' \qquad 3.3$$

$$H_y(\vec{r}_p,t)=\frac{1}{4\pi}\int\int\int_{V'}\frac{r_z J_h\sin\psi + r_x J_z}{|\vec{r}|^3}dV' \qquad 3.4$$

$$H_z(\vec{r}_p,t)=\frac{-1}{4\pi}\int\int\int_{V'}\frac{r_y J_h\sin\psi + r_x\cos\psi\, J_h}{|\vec{r}|^3}dV' \qquad 3.5$$

3.3 The pulsed field of a multi-turned coil.

Calculating the magnetic field of a multi-turned coil requires solving Eqns. 3.3 - 3.5 for each turn individually. Thus the limits of integration need to be adopted to describe each turn in the XYZ reference system. The limits are adopted as follows (see Fig 3.1):

i) To account for radial increases in alternatively fitted right and left handed helix coils, limits of integration for rho are changed to:

$$\rho \in [a + (w + g)helixnum - 1, a + (w + g)helixnum - g]$$

where: g - is he distance of possible airgaps existing between alternatively fitted helixes.

helixnum - integer $\in$ [1,n] with helixnum = 1 describing the innnermost helix.

ii) If each wire helix has m turns, the limits of integration for turn number $t \in [1,m]$ displaced in the +z axis direction of a right-handed helix is given by:

$$z \in \left[\frac{p}{2\pi}(\eta + (t-1)2\pi), \frac{p}{2\pi}(\eta + (t-1)2\pi) + h\right]$$

$$\eta = \psi \quad (\psi < 2\pi) \quad ; \quad \eta = 2\pi - \psi \quad (\psi > 2\pi)$$

Similarly the turns of a left-handed wire helix has the limits of integration for z changed to:

$$z \in \left[\frac{p}{2\pi}(2\pi t - \eta), \frac{p}{2\pi}(2\pi t - \eta) + h\right]$$

$$\eta = \psi \quad (\psi < 2\pi) \quad ; \quad \eta = 2\pi - \psi \quad (\psi > 2\pi)$$

iii) Limits of integration for psi are unchanged.

To account for a multi-turned coil Eqns 3.3 - 3.5 are written as:

$$H_x(\vec{r}_P, t) = \sum_{n=1}^{Helixes} \sum_{m=1}^{Turns} H_{xmn}(\vec{r}_P, t) \qquad 3.6$$

$$H_y(\vec{r}_P, t) = \sum_{n=1}^{Helixes} \sum_{m=1}^{Turns} H_{ymn}(\vec{r}_P, t) \qquad 3.7$$

$$H_z(\vec{r}_P, t) = \sum_{n=1}^{Helixes} \sum_{m=1}^{Turns} H_{zmn}(\vec{r}_P, t) \qquad 3.8$$

REFERENCES

[8] Wolfgang K.H. Panofsky and Melba Philips, Classical Electricity and Magnetism, Addison-Wesley Publishing company Inc, 1964, 2nd Edition, Pg. 246

4. EDDY CURRENT EFFECTS IN SOLID CONDUCTORS

Conductors carrying time varying currents are effected by a phenomenon called "Skin Effect". This phenomenon results in the time dependent current density being non-uniformly distributed over the conductor's cross-sectional area. The uneven current distribution also causes the impedance of the conductor to change, ie the resistive component of impedance increases, resulting in higher ohmic losses and greater heating in the conductor.

This chapter documents the results obtained, on application of an algorithm presented in papers [9] and [10], for solving the skin equation in conductor's having symmetrical cross-sectional areas.

4.1 Mathematical Summary.

From [9], the solution to the skin equation of conductor's having symmetrical cross-sectional areas (Fig. 4.1) is:

$$J_z(r_c,\phi_c) = \sigma \sum_{n=0}^{N} A_n I_{2n}(\alpha r_c)\cos[2n\phi_c]$$

where:

σ - Conductivity of the conductor

μ - Permeability of the conductor

α - $\sqrt{jw\sigma\mu}$

I_{2n} - Modified Bessel functions of order 2n

w - radial frequency of sinusoidal current

A_n - Calculated constants (see later)

and r_c, ϕ_c are spherical co-ordinates of points inside the conductor

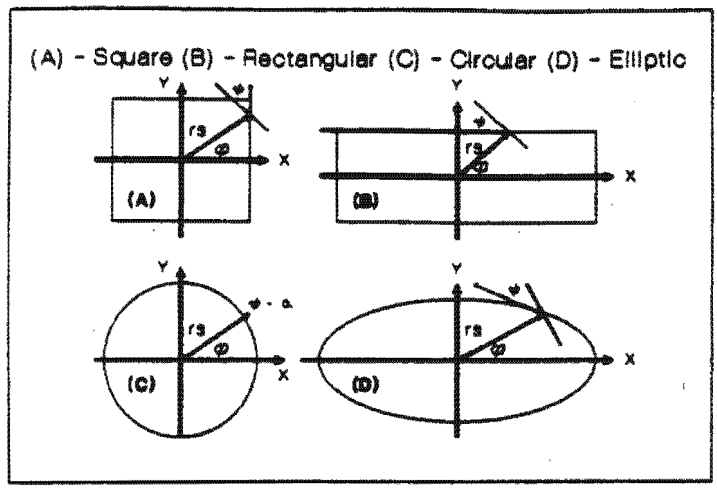

Figure 4.1 Conductors having symmetrical cross-sectional areas.

For each conductor the following is assumed:

i) The conductor's cross-sectional area is symmetrical about the XY axes and the conductor is infinitely long in the + - z axis directions.

ii) The Electric flux intensity both inside and outside the conductor has only a z vector component.

iii) A sinusoidal current $i(t) = I_o e^{-jwt}$ flows in the + z direction along the conductor.

Using the skin equation:

$$\left[\nabla^2 - \alpha^2\right] E_z = 0$$

Maxwell's equation:

$$\nabla \times \vec{E} = -j\mu\omega\vec{H}$$

and the boundary conditions applicable at the edge of the conductor, the solutions for the coefficients An is reduced to solving 2(N + 1) complex linear equations defined by:

$$\sum_{n=0}^{N}\left[A_n L^k_{1nml} + B_n L^k_{2nml}\right] = \alpha^k_{ml} \qquad 4.1$$

where:

$k = 1,2 \quad m = 0,1,2..M_1 \quad l = 1,2,..L$

$$a_{ml}^{(k)} = \int_{\phi_{l-1}}^{\phi_l} F^k \cos[2m\phi_c]\partial\phi_c$$

$$L_{1mnl}^{(k)} = \int_{\phi_{l-1}}^{\phi_l} \phi_{1n}^k \cos[2m\phi_c]\partial\phi_c$$

$$L_{2mnl}^{(k)} = \int_{\phi_{l-1}}^{\phi_l} \phi_{2n}^k \cos[2m\phi_c]\partial\phi_c$$

$$\phi_{1n}^{(1)} = I_{2n}[\alpha r_s]\cos[2n\phi_c]$$

$$\phi_{2n}^{(1)} = -\frac{\cos[2n\phi_c]}{r_s^{2n}}$$

$$* \quad \phi_{1n}^{(2)} = \mu_0[\alpha r_s I'_{2n}(\alpha r_s)\cos[2n\phi_c] - 2n I_{2n}(\alpha r_s)\tan\psi_c \sin[2n\phi_c]/\mu$$

$$* \quad \phi_{2n}^{(2)} = 2n[\cos[2n\phi_c] + \tan\psi_c \sin[2n\phi_c]/r_s^{2n}$$

$$F^{(1)} = \xi \ln[r_s]$$

$$F^{(2)} = \xi$$

$$\xi = j\omega\mu_0 \frac{I}{2\pi}$$

$$\psi_c = -\arctan\left[\frac{1}{r_s}\partial\frac{r_s}{\partial\phi_c}\right]$$

and:

I_2n – Derivative of the Modified Bessel function.

– Angle between the azimuthal direction and the tangent to the conductor at a given point.

rs – Distance from the center of the conductor to the outer edge (not necessary constant eg Square conductors)

I – Instantaneous current

* *The signs of these equations in both papers [9] and [10] are incorrect.*

The circumference of the conductor's cross-section is divided into L segments. The integration from ϕ_{l-1} to ϕ_l is carried out along the l'th segment. It is important that values of M_l and L are chosen so that the number of equations equals the number of unknown coefficients. Values of M_l and L are chosen depending on the convergence of the series Eqn. 4.1 and the distribution of the current across the conductor cross section.

4.2 Non-Uniform Current Distributions

The skin equation algorithm was applied to each of the conductor shapes illustrated in Fig.4.1. Various characteristics of current density distribution are shown, by using different modes of display, for each conductor cross-sectional area.

4.2.1. Elliptical Conductor.

The current density distribution was calculated at several points inside the Elliptical conductor shown in Fig. 4.2a.

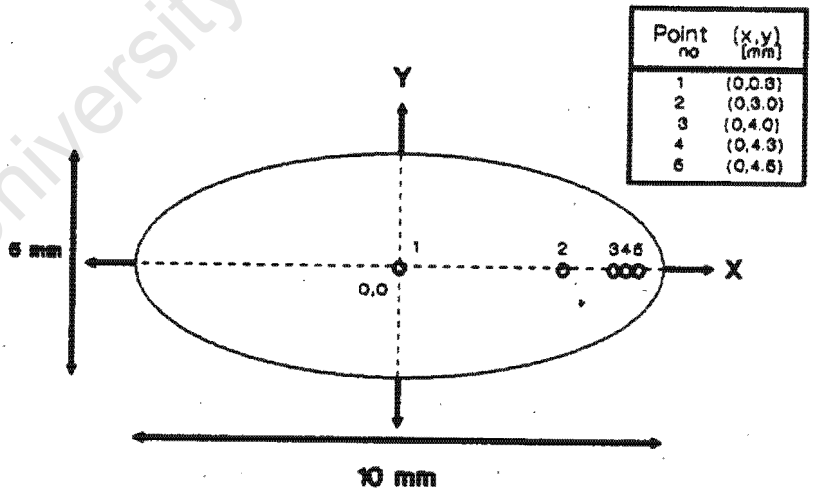

Figure 4.2a Elliptical Conductor.

Results:

The results are plotted as a function of frequency for each point (Fig. 4.2b).

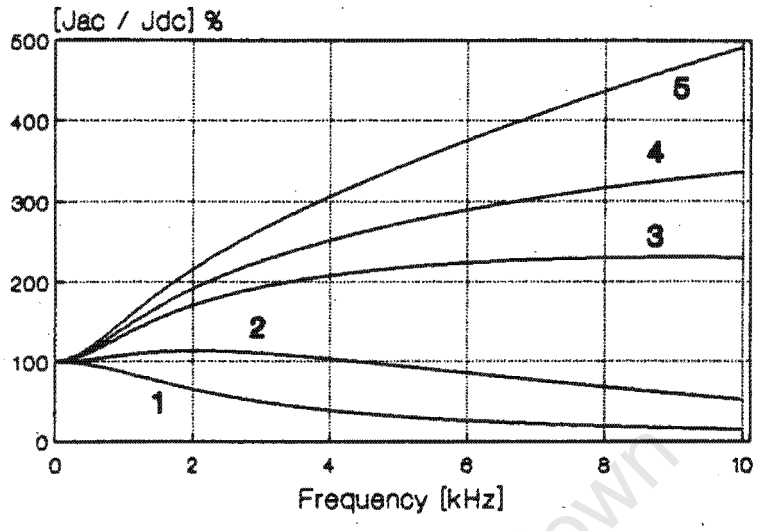

Figure 4.2b Current Density at points 1-5 inside the Elliptical conductor of Figure 4.2a versus frequency.

i) At Dc and lower frequencies (0-100hz), the current density is approximately equal to the Dc value for all the points.

ii) With increase in frequency, the current density in the region of the conductors center tends to zero (pt1).

iii) The current density increases at points nearer the conductors edge for higher frequencies. The rate of increase is greater for points closer to the boundary.

iv) At each point inside a conductor, there is a unique frequency at which a maximum value of current density is realised. Upon reaching this value, a continued increase in frequency causes the current density to decrease (pt2).

4.2.2. Rectangular Conductor.

The current distribution was calculated along the:

i) diagonal of the rectangular conductor (Fig 4.3a) for frequencies 1 Khz, 10 Khz and 1 Mhz.

ii) diagonals of square connductors having cross-sectional areas of 1 mm^2, 10 mm^2, 100 mm^2 at a frequency of 3 Khz.

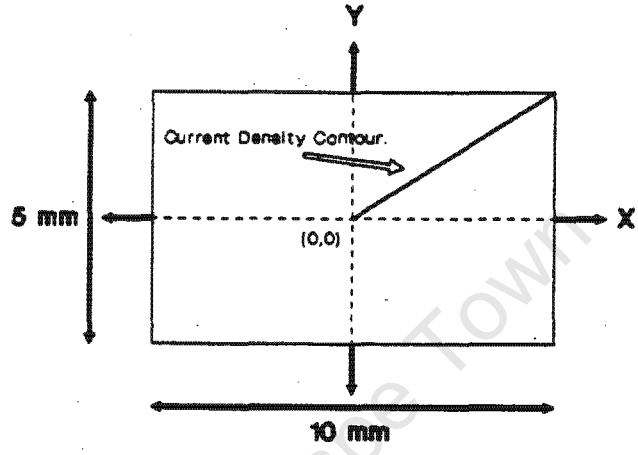

Figure 4.3a Cross-Section of a Rectangular conductor.

Results:

i) With increase in frequency, the current density becomes more concentrated at the conductors edge and approaches a skin current (Fig 4.3b).

ii) Current distribution is related to conductor size and becomes more unevenly distributed with increase in conductor cross-sectional area (Fig. 4.4).

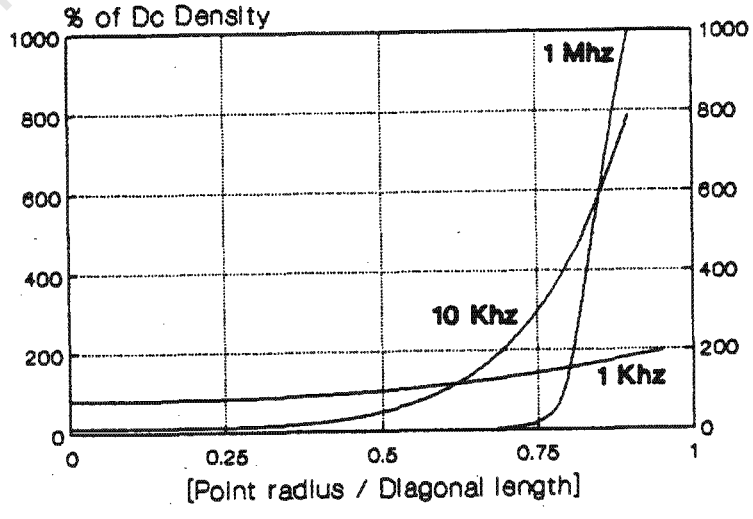

Figures 4.3 b Current density along the diagonal of a Rectangular conductor for frequencies 1 Khz,10 Khz and 1 Mhz.

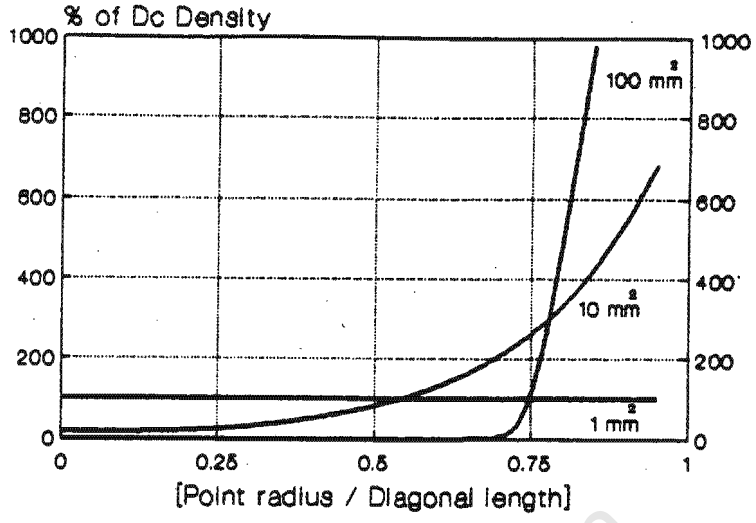

Figure 4.4 Current distribution along the diagonal contour of different square conductors at 3Khz.

4.2.3. Circular conductor.

The 100% current density contour (ie equal to the Dc value) was calculated inside a circular conductor at frequencies of 1Khz, 10Khz and 100Khz (Fig 4.5).

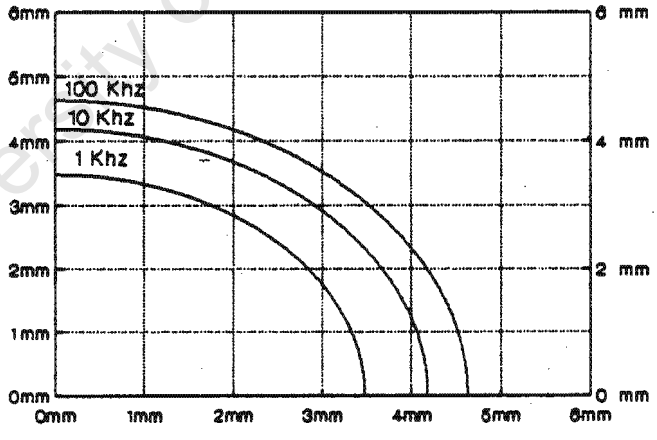

Figure 4.5 The position of the 100% current density contour inside a circular conductor (radius = 5mm) at different frequencies.

From figure 4.5:

- The density contours are circular
- Constant density contours move symmetrical towards the conductors edge with increasing frequency.

4.3 Impedance of a Solid Conductor.

The non-uniform distributions of current density results in a change of conductor impedance. Using the method discussed in [9] and [10], the internal impedance per unit length of a long conductor at some frequency is given by:

$$+ \quad Z = -\frac{4}{j\omega\mu}\sum_{n=0}^{N}\sum_{m=0}^{N} A_n A_m^{*}\left[X_{nm} - \Gamma_{nm}\right] \qquad 4.2$$

with:

$$X_{nm} = \int_0^{\pi/2} I_{2n}[\alpha r_s]\cos[2n\phi_c]\cos[2m\phi_c]\alpha^{*} r_s I'_{2m}[\alpha^{*} r_s]\partial\phi_c$$

$$\Gamma_{nm} = \int_0^{\pi/2} I_{2n}[\beta r_s]\cos[2n\phi_c]\sin[2m\phi_c] I_{2m}[\beta^{*} r_s] 2m\tan\psi_c\partial\phi_c$$

and all other variables are as defined in section 4.1.

To illustrate the effect of changing conductor impedance with frequency, Eqn. 4.2 was solved for two rectangular conductors having different cross-sectional areas. Resultant plots of resistance and reactance normalised to each conductors unique DC resistance are shown in figures 4.6a and 4.6b, where. the DC resistance per unit length of a rectangular conductor is given by:

$$R_{dc} = \frac{1}{width \cdot height \cdot \sigma}$$

+ Equation 4.1 has a different format to that given in [9] and [10].

Results:

i) Reactance and resistive components of impedance are frequency dependent. (ie they vary in magnitude from the Dc values)

ii) The change in impedance is greater for the conductor with largest cross -sectional area.

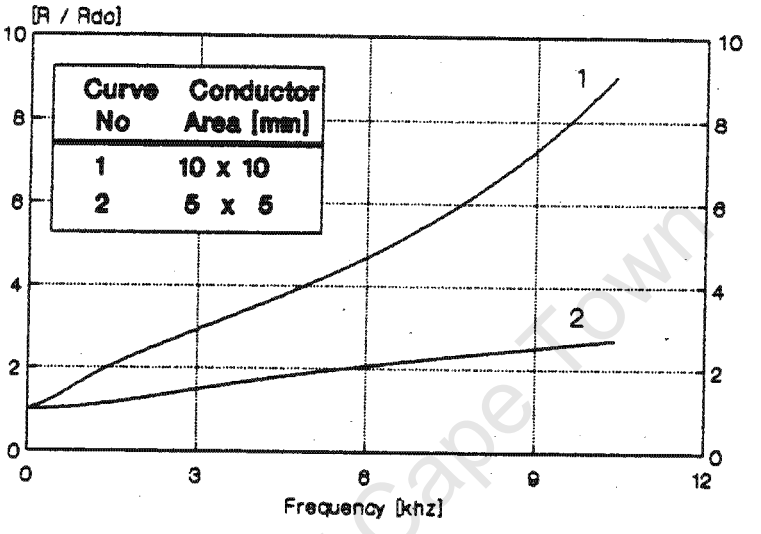

Figure 4.6a Conductor normalised resistance R/Rdc versus frequency

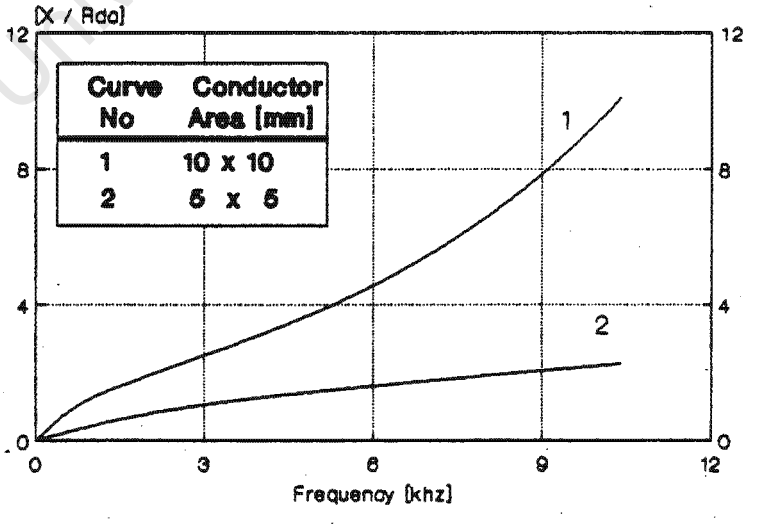

Figure 4.6b Conductor normalised reactance X/Rdc versus frequency

All results of application of the algorithm presented in papers [9] and [10] are in agreement with expectations. The algorithm accurately approximates the characteristic skin-effect behavior inside 2D conductor planes. If this approximation is assumed to occur throughout 3D volumetric conductors, then eddy current effects can be approximated inside physical 3D conductors.

REFERENCES

[9] A.M. Hussein and P.P. Biringer, "Current Distributions in Conductors with Arbitrary Cross Sections", IEEE Trans on Magn, Vol Magn-22, No 5, September 1986, Pg 1263-1265.

[10] A.M Hussein and P.P Biringer, "Applications of the Boundary Matching Method to Elliptic Conductors", J. Appl.Phys, Vol 60, No 9, Nov 1986, Pg 3357-3359.

5. PULSED MAGNETIC FIELD

With the analysis from chapter 3, the method used to solve the pulsed magnetisation field for the helical coil turn model is described in this chapter.

5.1 Eddy Current Losses.

Eddy current losses on the magnetisation field were accounted for by applying the " Eddy Loss" algorithm described in chapter 4. If it is assumed that current distributions calculated in the 2D plane is also valid throughout the model coil volume, the "skin effect" characteristics are approximated inside the coil.

5.1.1 Changing coil impedance.

When solving the complex conductor impedance Eqn 4.2 in chapter 4, it is evident from the results that both resistive and reactive components are frequency dependent. Eqn 4.2 has to be solved separately at each discrete frequency value, to calculate impedance. For this reason and because of it's complexity, it is impractical to use this equation directly in determining the effects of changed impedance on magnetic field.

The results of Eqn 4.2 however can be used to synthesis a new equivalent circuit for the coil.[11] A series LR network is the DC coil equivalent circuit. This circuit was used in chapter 2 to derive the magnetising current pulse. However to account for the new AC effects, the coil impedance was assumed to be:

$$Z_{AC} = \frac{R_{DC}\,\beta_1\left[s+\alpha_1\right]\left[s+\alpha_2\right]}{\alpha_1\,\alpha_2\left[s+\beta_1\right]} \qquad 5.1$$

with:

w = radial frequency, $s = jw$, $\alpha 1, \alpha 2$ = zero's of the network and $\beta 1$ = network pole.

Values of the network zero's and pole, are calculated to give the best approximation to the impedance curve. The equivalent circuit for Zac is synthesised to a parallel connection of two RL series networks where:

$$L_1 = R_{DC}\,\beta_1 \frac{[\alpha_2 - \alpha_1]}{\alpha_1 \alpha_2 [\beta_1 - \alpha_1]} \qquad R_1 = \alpha_1 L_1$$

$$L_2 = R_{DC}\,\beta_1 \frac{[\alpha_1 - \alpha_2]}{\alpha_1 \alpha_2 [\beta_1 - \alpha_2]} \qquad R_2 = \alpha_2 L_2$$

The accuracy of approximating the impedance equation, is dependent upon the bandwidth of the curve of be fitted, and the degree of curve variation. In general all magnetising pulses have a time duration of greater than 6 milliseconds, and thus it was assumed a bandwidth of within 5khz. Thus Eqn 5.1 is required to approximate Eqn 4.3 to within a bandwidth of 5 Khz. Fig 5.1 shows the results of fitting Eqn 5.1 to the resistance curve of a 100-turned coil made from 28 meters of wire. The conductor's cross-sectional area was 1.45mm x 7.5 mm and the DC inductance measured was 197 microHenries. The figure shows clearly that to within a bandwidth of 5Khz a good approximation is obtained. The initial coil reactance was only slightly changed by "skin-effect" and the equivalent circuit fitted this curve exactly In general a fit to within 10% error of any conductor impedance curve was possible within a bandwidth of 5 Khz.

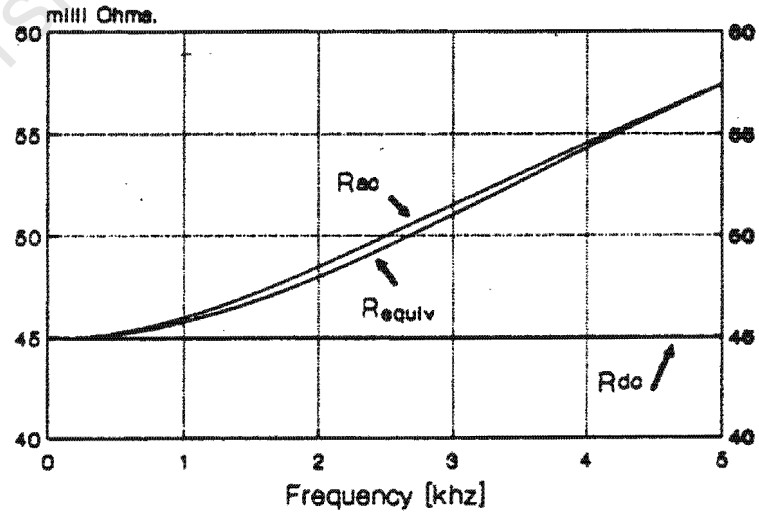

Figure 5.1 Approximation of the Ac resistance due to skin effect by an equivalent circuit. $\alpha 1 = 227$, $\alpha 2 = 37855$, $\beta 1 = 37699$, L1 = 199 μH, R1 = 45 milliOhms, L2 = 42.8 H, R2 = 1082.3 milliOhms

To fit an impedance curve of greater bandwidth, Eqn. 5.1 must be modified which results in a more complex equivalent circuit for the coil.

5.1.2 Current equations.

Using the new equivalent circuit for the coil, the magnetising circuit of chapter 2 is changed to the circuit shown in Fig 5.2.

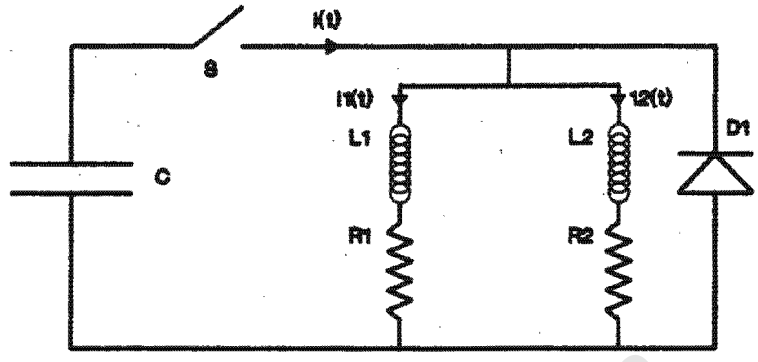

Figure 5.2 Magnetising circuit which includes the changed equivalent coil impedance (L1,L2,R1,R2) due to skin effect. At t = 0 the capacitor bank (C) voltage = V_o. D1 is the Free-wheel diode

As in chapter 2, the total current flowing through the coil is described separately by different equations before and after the free-wheel diode conducts. To determine these currents, Fig 5.2 is redrawn as a second equivalent circuit (Fig 5.3).

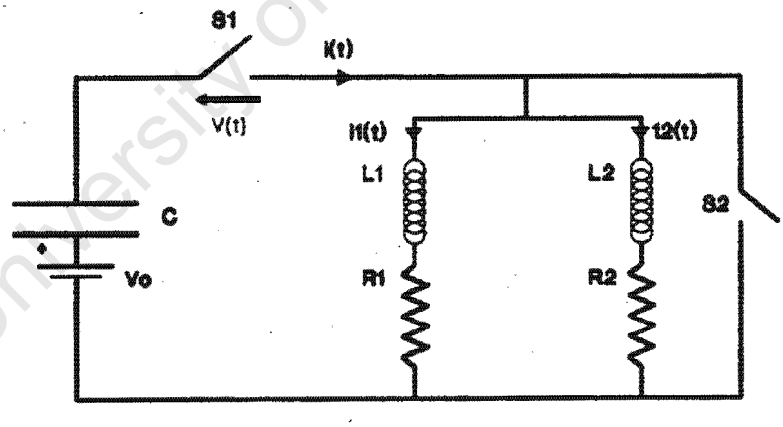

Figure 5.3 Equivalent Magnetising circuit of Fig 5.2 used to determine the current flowing through the new equivalent coil.

The capacitor with an initial charge V_o is replaced by a capacitor with no initial charge in series with a constant voltage V_o. Also the free-wheel diode is replaced with a selective switch that is closed for forward voltages and open for reverse voltages.

At time = 0, switch S1 is closed. The system equations are:

$$\frac{1}{C}\int\left[i_1(t)+i_2(t)\right]\partial t - V(t) + R_1\ i_1(t) + L_1\ \partial i_1\frac{(t)}{\partial t} = 0$$

$$\frac{1}{C}\int\left[i_1(t)+i_2(t)\right]\partial t - V(t) + R_2\ i_2(t) + L_2\ \partial i_1\frac{(t)}{\partial t} = 0$$

with the conditions:

$$V(t<0) = V_o\ , V(t>=0) = 0 \text{ and } i(0) = 0.$$

Using Laplace transforms, currents $i_1(t)$ and $i_2(t)$ are written in the S-plane as:

$$I_1(s) = \frac{V_0\left[s + R_2/L_2\right]}{L_1\left[s^3 + s^2\left[\frac{R1}{L1}+\frac{R2}{L2}\right] + s\left[\frac{1}{L_1C}+\frac{1}{L_2C}+\frac{R_1R_2}{L_1L_2}\right]+\frac{R1+R2}{L1L2C}\right]} \qquad 5.2$$

$$I_2(s) = \frac{V_0\left[s + R_1/L_1\right]}{L_2\left[s^3 + s^2\left[\frac{R1}{L1}+\frac{R2}{L2}\right] + s\left[\frac{1}{L_1C}+\frac{1}{L2C}+\frac{R1R2}{L1L2}\right]+\frac{R1+R2}{L1L2C}\right]} \qquad 5.3$$

where $I_1(s)$ and $I_2(s)$ are the transforms of $i_1(t)$ and $i_2(t)$. From Eqn 5.2, Eqn 5.3 and Fig 5.3 the coil current is given by:

$$i(t) = L^{-1}\left[\frac{\frac{V_o}{L1}\left[s + R_2/L_2\right] + \frac{V_o}{L2}\left[s + R_1/L_1\right]}{\left[s^3 + s^2\left[\frac{R1}{L1}+\frac{R2}{L2}\right] + s\left[\frac{1}{L1C}+\frac{1}{L2C}+\frac{R1R2}{L1L2}\right]+\frac{R1+R2}{L1L2C}\right]}\right] \qquad 5.4$$

Writing the denominator of Eqn 5.4 as $[(s + a)^2 + b^2][s + c]$, with constants a,b,and c solved numerically, i(t) can be solved from the following Laplace Transform formula [12]:

$$\frac{s+a_0}{[(s+a)^2+b^2][s+c]} \Leftrightarrow A_1 \exp[-at]\sin[bt+v_1]+\frac{[a_0-c]\exp[-ct]}{[a-c]^2+b^2}$$

$$A_1 \angle v_1 = \frac{a_0-[a-jb]}{b[c-a+jb]}$$

as:

$$i(t<t_{peak}) = i_1(t)+i_2(t) \qquad 5.5$$

$$i_1(t) = \frac{V_0}{L1}\left[A_1 \exp[-at]\sin[bt+v_1]+\frac{\left[\frac{R2}{L2}-a+jb\right]\exp[-ct]}{b[c-a+jb]}\right]$$

$$i_2(t) = \frac{V_0}{L2}\left[A_2 \exp[-at]\sin[bt+v_2]+\frac{\left[\frac{R1}{L1}-a+jb\right]\exp[-ct]}{b[c-a+jb]}\right]$$

Eqn. 5.5 defines the coil current i(t) until a time t_{peak} when the free-wheel diode starts conduction. From Fig. 5.2 this is equivalent to closing S2 at t_{peak}. Circuit equations that now apply are:

$$L_1 \frac{\partial i_1(t)}{\partial t}+i_1(t)R_1 = 0$$

$$L_2 \frac{\partial i_2(t)}{\partial t}+i_2(t)R_2 = 0$$

with: $V_{capacitor} = 0$ for $t > t_{peak}$

Again by using Laplace transformations, the coil current is solved to:

$$i(t \geq t_{peak}) = I_{peak1}\exp\left[-\frac{tR_1}{L_1}\right]+I_{peak2}\exp\left[-\frac{tR_2}{L_2}\right] \qquad 5.6$$

Time t_{peak} is the time when the derivative of 5.5 is zero ie:

$$\frac{\partial i(t)}{\partial t} = \frac{\partial i_1(t)}{\partial t} + \frac{\partial i_2(t)}{\partial t} = 0 \qquad t < t_{peak} \qquad 5.7$$

$$\frac{\partial i_i(t)}{\partial t} = \frac{V_0}{Li}\left[-aA_i\exp[-at]\sin[bt+v_i] + bA_i\exp[-at]\cos[bt+v_i] - \frac{c\left[\frac{Ri}{L} - a + jb\right]\exp[-ct]}{b[c-a+jb]}\right] \qquad i = 1,2$$

Because of the complexity of Eqn. 5.7, a numerical method was used to find t_{peak}. Constants I_{peak1} and I_{peak2} of Eqn. 5.6 are the values of $i_1(t)$ and $i_2(t)$ at time t_{peak}.

5.1.3 Accounting for non-uniform current distributions.

Sections 5.1.1 and 5.1.2 have described how the effect on current of changing coil impedance do to "Skin Effect", has been compensated. This section describes how the non-uniform current distributions in the coil are taken into account.

For simplicity of mathematical analysis, it was assumed that the magnetising current pulse (including the new coil equivalent circuit), is periodic with duration T_{period}. A discrete frequency spectrum of the magnetising pulse can now be obtained by calculating the Fourier series of this pulse. This spectrum is an approximation of the continuous spectrum and becomes more accurate the larger the period is assumed to be. From [13], the current pulse is expressed in terms of the complex Fourier series c_k as:

$$i_{periodic}(t) = C_0 + 2\sum_{k=1}^{N} |C_k| \cos\left[\frac{2\pi kt}{T_{period}} + Arg[C_k]\right] \quad 5.8$$

where, $|C_k|$ and $Arg[C_k]$ are absolute value and argument of C_k respectively,ie:

$$|C_k| = \frac{\sqrt{a_k^2 + b_k^2}}{2} \qquad Arg[C_k] = \arctan\left[-\frac{b_k}{a_k}\right]$$

and:

$$C_0 = a_0 = \frac{1}{T_{period}}\int_0^{T_{period}} i(t)\,\partial t$$

$$a_k = \frac{2}{T_{period}}\int_0^{T_{period}} i(t)\cos\left[\frac{2\pi kt}{T_{period}}\right]\partial t$$

$$b_k = \frac{2}{T_{period}}\int_0^{T_{period}} i(t)\sin\left[\frac{2\pi kt}{T_{period}}\right]\partial t$$

$i(t<t_{peak})$ defined by Eqn. 5.5

$i(t>t_{peak})$ defined by Eqn. 5.6

N - n'th frequency harmonic

Using the principles of superposition and Eqn. 5.8, the total magnetic field at any point outside the conductor, is the summation of field contributions from each of the harmonic current components considered separately. Thus Eqns 3.6 - 3.8 are modified to:

$$H_x(\vec{r}_p,t)=\sum_{n=1}^{Helixes}\sum_{m=1}^{Turns}\left[H_{0x}+\frac{1}{2\pi}\sum_{k=1}^{N}\int\int\int_{Vmn'}\frac{r_z J_{hk}\cos\psi - r_y J_{zk}}{|\vec{r}|^3}dV_{nm}'\right] \quad 5.9$$

$$H_y(\vec{r}_p,t)=\sum_{n=1}^{Helixes}\sum_{m=1}^{Turns}\left[H_{0y}+\frac{1}{2\pi}\sum_{k=1}^{N}\int\int\int_{Vnm'}\frac{r_z J_{hk}\sin\psi + r_x J_{zk}}{|\vec{r}|^3}dV_{nm}'\right] \quad 5.10$$

$$H_z(\vec{r}_p,t)=\sum_{n=1}^{Helixes}\sum_{m=1}^{Turns}\left[H_{0z}-\frac{1}{2\pi}\sum_{k=1}^{N}\int\int\int_{Vnm'}\frac{r_y J_{hk}\sin\psi + r_x\cos\psi\, J_{hk}}{|\vec{r}|^3}dV_{nm}'\right] \quad 5.11$$

where:

$$\vec{J}_{wk}=\vec{J}_k(\vec{r}_Q)\cos\left[\frac{2\pi kt}{T_{period}}+Arg[C_k]\right]$$

$$J_{hk}=|\vec{J}_{wk}|\cos\gamma \qquad J_{zk}=|\vec{J}_{wk}|\sin\gamma$$

and H_{ox}, H_{oy}, H_{oz} are static magnetic field vector components obtained from:

$$\vec{H}_0=\frac{1}{4\pi}\int\int\int_{Vnm'}\frac{\vec{J}\times\vec{r}}{|\vec{r}|^3}dV'_{nm} \quad 5.12$$

Using the "Skin Effect" algorithm described in chapter 4, it is possible to solve the current distribution vector $\vec{J}_k(\vec{r}_Q)$ for each spectral harmonic of the magnetising pulse. Thus the time-dependent non-uniform current distribution is taken into account.

A intuitive simplification is possible if the eddy current losses are considered insignificant and are neglected. The current density vector for this case is given by:

$$J(t) = \frac{i(t)}{[conductor \;\; cross-sectional \;\; area]} \qquad 5.13$$

Equation 5.13 stipulates that $\vec{J}(\vec{r_Q})$ is uniformly distributed on the conductor's cross-sectional plane at any time instance. The magnitude however is time-dependent, proportional to current changes i(t) defined by Eqns 2.1 and 2.2. Thus only Eqn. 5.12 applies for the field with the current density J given by Eqn. 5.13. This approximation allows a comparison between field results with or without eddy current losses and offers an insight into field losses due to "skin effect".

5.2 Numerical Solution.

To solve Eqns 5.9 - 5.11, 3D integration must be performed over the volume of the model helical coil turn for each frequency of the field. This calculation is repeated for each winding of the nxm turned coil. An analytical solution is not possible because of the integrals complicated nature, so the integration is solved using Gauss Legendre Quadrature. [14] This technique of integration is used because of it's numerous advantages. These are fast computational speeds, different modes of accuracy and it's easy adoption to solving a definite integral problem, compared to most other numerical techniques.

If no singularities exist between the limits of integration, (which is true for Eqns. 5.9 - 5.11, providing the field point is outside the conductor) a function `f(x,y,z)` is approximated using Gauss Quadrature, by an n'th degree interpolating orthogonal polynomial. The integration of `f(x,y,z)` over 3D is approximated by:

$$\int_{a3}^{b3}\int_{a2}^{b2}\int_{a1}^{b1} f(x,y,z)\,dx\,dy\,dz \;\equiv\; F[\zeta,\xi,\chi] \qquad 5.14$$

where:

$$F[\xi,\xi,\chi] = \frac{(b3-a3)(b2-a2)(b1-a1)}{2^3}\sum_{i=1}^{n}\sum_{j=1}^{n}\sum_{k=1}^{n} W_i W_j W_k \Omega[\xi,\xi,\chi]$$

$$\Omega[\xi,\xi,\chi] = f\left[\frac{x_i(b1-a1)+b1+a1}{2}, \frac{y_j(b2-a2)+b2+a2}{2}, \frac{z_k(b3-a3)+b3+a3}{2}\right]$$

W_i, W_j, W_k weight factors for roots x_i, y_j, z_k obtained from tables

Equations 5.9 - 5.11 used in conjunction with Eqn. 5.14 are solved with the aid of a computer. Fig. 5.4 (see next page) shows a flowchart of the entire numerical analysis in logical layout. To avoid excessive numerical repetitions and large calculations times, several computational saving techniques were used and the calculations were not solved strictly in the sequence shown by Fig. 5.4 The time dependent field results were displayed as a vector (H_x,H_y,H_z) for different spatial points and time instances.

REFERENCES

[11] Lovis Weinberg, Network Analysis and Synthesis, McGraw-Hill Book Company Inc, 1962

[12] Gladwyn V. Lago and Donald L. Waidelich, Transients in Electrical Circuits, The Ronald Press Company, New York, 1958.

[13] NezIH C. Geckinli and Darvis Yavuz, Discrete Fourier Transformations and it's Application to Power Spectra Estimation, Elsevier Scientific Publishing company, 1983.

[14] A.H.Stroud and Don Secrest, Gaussian Quadrature Formulas.

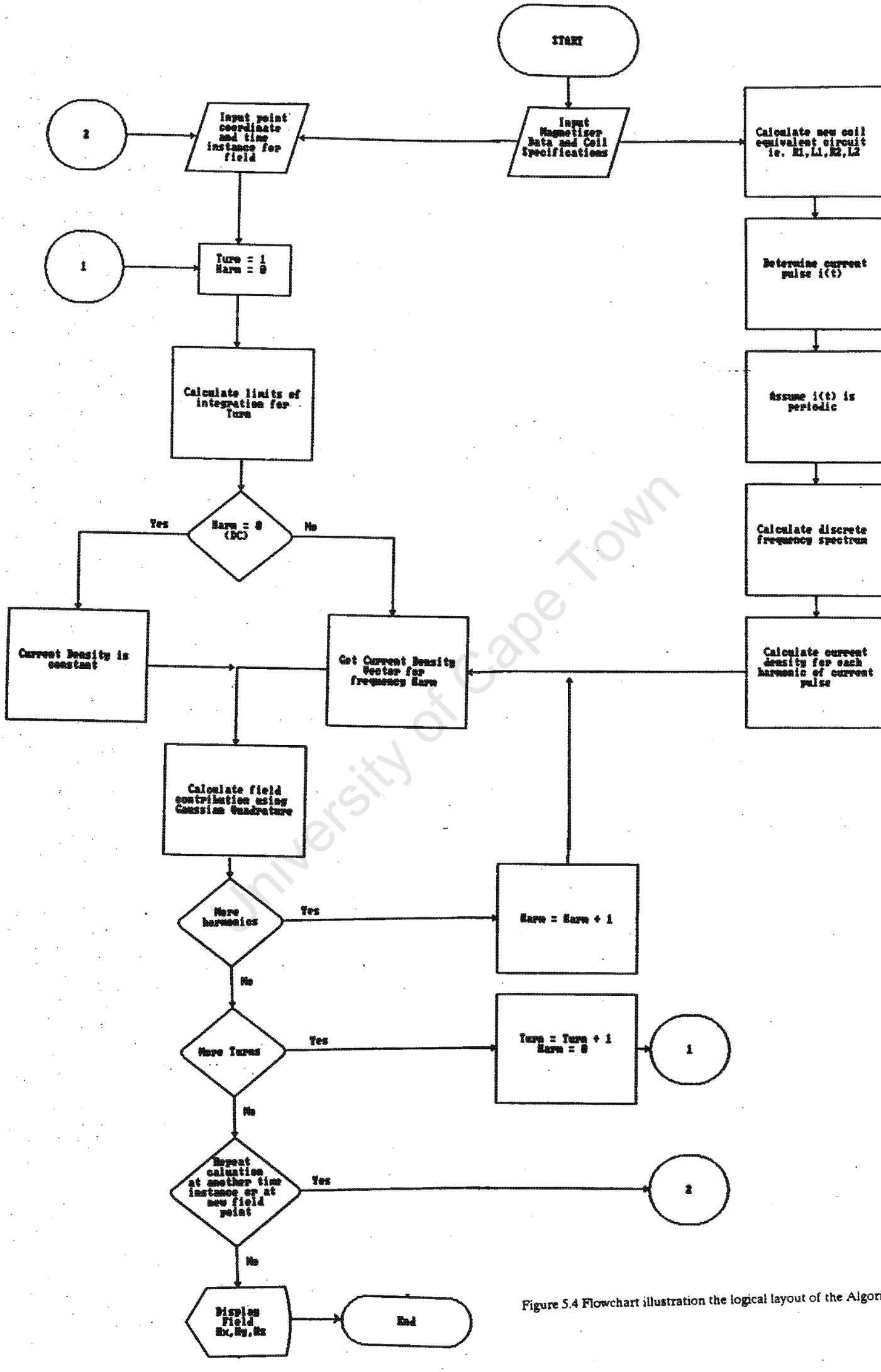

Figure 5.4 Flowchart illustration the logical layout of the Algorithm.

6 COMPARISON OF RESULTS.

The time dependent field intensity of a current carrying conductor is not readily solvable by analytical methods. This severely limits the number of available methods to check the algorithm. For the magnetostatic field, hypothetical coils such as the Torroid, where analytical solutions are available, were used to check the predicted field magnitude and behavior. Also the field was calculated along several contours of coils at which the field behavior could be predicted. The only method to check the accuracy of the predicted versus actual pulsed field was by measurements. Due to limited project funding, a Gaussmeter with sufficient bandwith was "self-constructed" and this limited the accuracy of the measured time-dependent results to + - 10% error.

6.1 The Magnetostatic Field of a Torroid

By assuming the pitch of the model helical coil turn is zero, the hypothetical current loop of Fig. 6.1 is approximated called a Torroid.

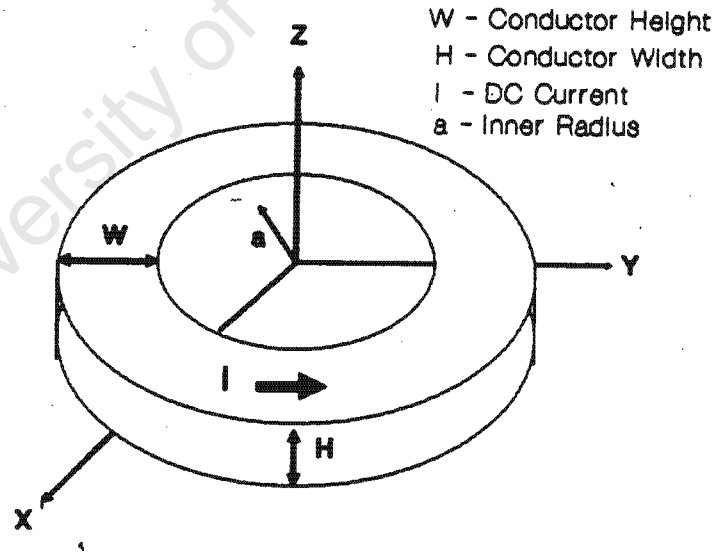

Figure 6.1 Torroidal Conductor.

A]

Considering only Eqn. 5.12, the magnetostatic field of a Torroidal conductor:

i) having dimensions similar to the example Torroid described in [15],

ii) having an infinitely thin cross-sectional area similar to the current loop in [16]

was calculated at:

i) identical points used in the example in [15],

ii) several random points above the current loop,

and the results compared to the analytical solutions given in both cases.

Results:

The results of the comparison are listed in:

i) Table 1

ii) Table 2

A good correlation between the analytical and calculated values of field is evident from the tables.

Point Coordinate [mm] (x,y,z)	Magnetic Field Intensity [A/m] Analytical	Calculated
(0,0,2.5)	38.08	38.08
(0,48,3.5)	163.67	152.55
(60,0,3.5	61.86	66.98
(0,57,4.5)	106.26	93.03
(48,0,5.5)	141.67	140.06
(0,80,3.5)	10.06	9.98
H = 5mm	W = 5mm a = 50mm	I = 4amps

TABLE1

Point Coordinate [mm] (x,y,z)	Magnetic Field Intensity [A/m] Analytical Hx	Hz	Calculated Hx	Hz
(5,0,0)	0.0	426.99	-0.34	426.77
(15,0,0)	0.0	765.21	-4.32	782.09
(10,0,10)	104.8	281.19	104.76	282.29
(20,0,10)	215.04	107.49	213.68	111.30
(20,0,20)	74.13	62.35	74.33	62.66
(25,0,30)	31.72	25.38	31.82	25.45
(30,0,38)	17.78	13.60	17.83	13.63
(40,0,50)	8.33	5.58	8.35	5.58
H = 0	W = 0	a = 20mm	I = 16.3amps	

TABLE2

B]

The magnetostatic field was calculated:

i) along radial axes of the z-plane bisecting the Torroidal conductor in half (Fig. 6.2). This calculation was repeated for several Torroidal conductor's of different cross-sectional area dimensions.

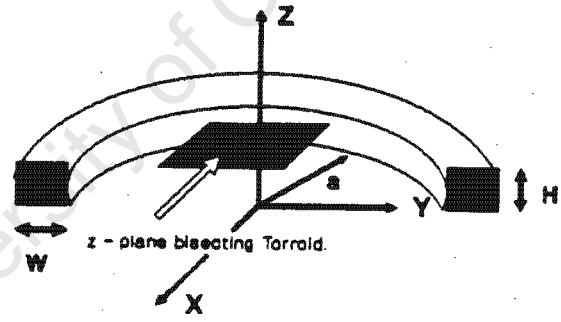

Figure 6.2 Cross-sectional view through a Torroid showing the bisecting plane.

ii) along radial axes of a z-plane that was positioned above the Torroidal conductor (Fig 6.3).

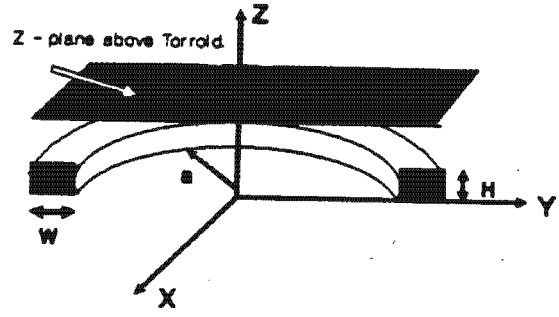

Figure 6.3 Cross-sectional view through a Torroid showing a typical z-plane above the Torroid.

Results:

i) For each Torroidal conductor, the magnetic field on the center plane:

i.1) is identical along all radii.

i.2) has only a Hz component of field. Both Hx and Hy are zero.

i.3) has a minimum a the Torroid center and increases symmetrically outwards (Fig 6.4).

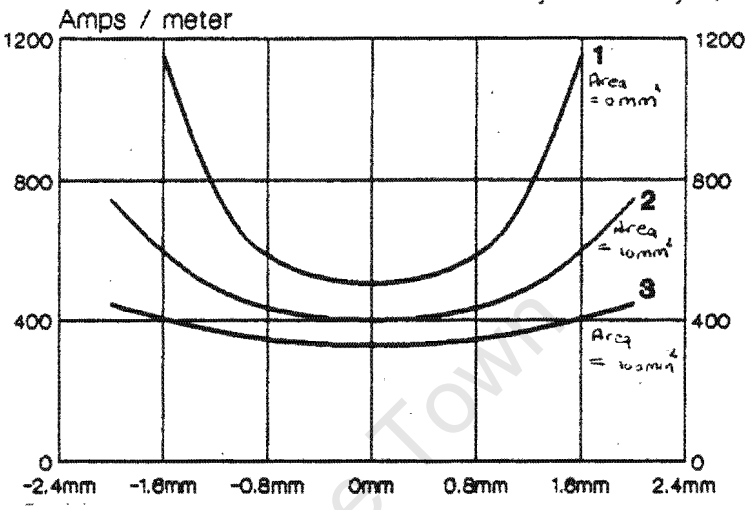

Figure 6.4 Field component Hz on the center plane of several Torroidal conductors. a = 20mm, I = 20A

i.4) decreases in strength (more noticeable nearer the conductor) with increase in cross-sectional area.

ii) The magnetic field in the z-plane above the conductor surface of the Torroid:

ii.1) has Hz and H components similar to those shown graphically in figures 6.5a and 6.5b. The field contour is dependent on the Torroid dimensions and the position of the z-plane.

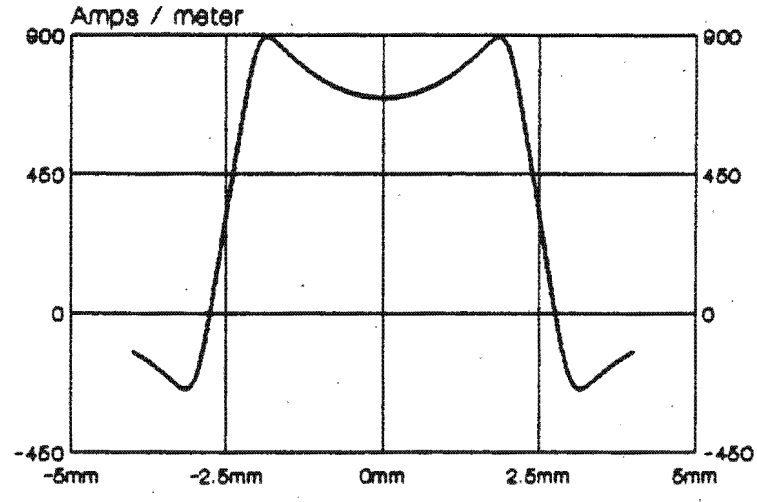

Figure 6.5a Hz field component in a plane above the Torroidal conductor having the following dimensions: a = 20mm, H = 10mm, W = 10mm.

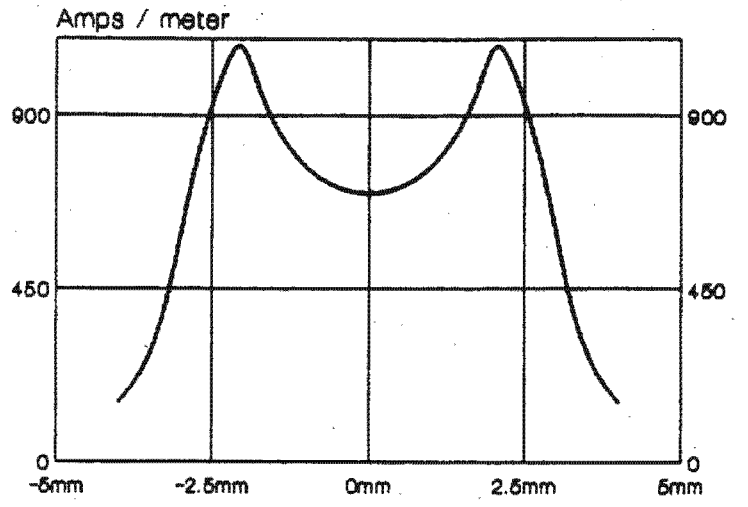

Figure 6.5b Field intensity H in a plane above the Torroidal conductor having the following dimensions: a = 20mm, H = 10mm, W = 10mm.

ii.2) has an Hz component of field that has an opposite vector direction inside the torroid to outside.

ii.3) has a radial field component that has two maxima of opposite vector directions. These maxima are above the conductors center on opposite sides of the Torroid (figure 6.5 c).

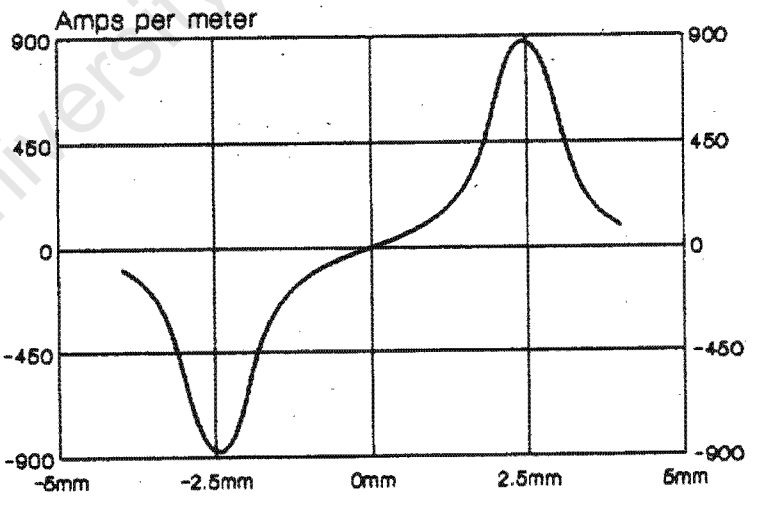

Figure 6.5c Radial field component in a plane above the Torroidal conductor having the following dimensions: a = 20mm, H = 10mm, W = 10mm.

These results are in agreement with what is expected by intuition and Flemings right-hand rule.

6.2 Fields of Multi-turned Coils.

Multi-turned coils can be approximated by the assemble of numerous model helical coil turns. Using this idea, the magnetic field (static and pulsed) was calculated for several coil configurations and the results compared to those measured or calculated, (where possible) by analytical methods.

A]

The magnetostatic field was calculated at several points on the z_axis of an N-turned helical coil having a small cross-sectional area (Fig. 6.6). Table 3 lists a comparison between the field measured and calculated by the analytical solution from [17], at several points of different dimensioned coils. An excellent agreement is evident.

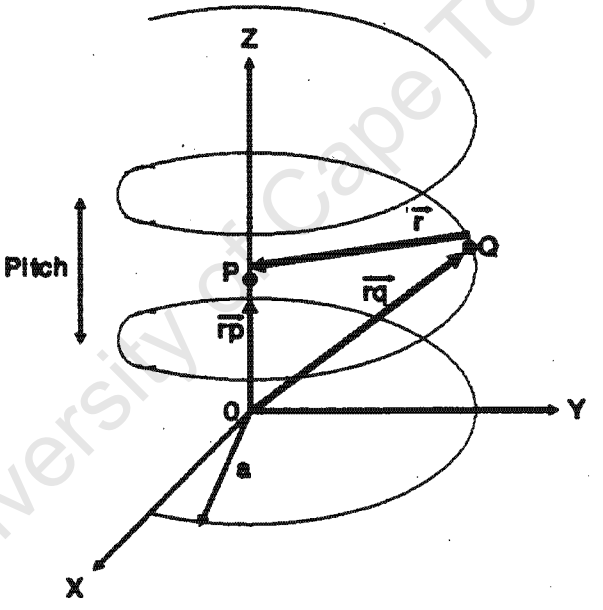

Figure 6.6 Helical coil having a small cross-sectional area.

z [cm] (x=0,y=0)	Turns	Radius [cm]	Pitch [cm]	Magnetic Field [A/m] Analytical	Calculated
0	1	11	5	67.33	67.28
3	5	11	5	188.33	187.91
8	10	11	5	253.09	252.48
6	1	11	10	52.92	52.91
7	1	10	10	47.97	47.96
1	5	10	10	383.07	383.072
Dc Current = 16.3 amps.					

TABLE 3

B]

A coil having 14 x 8 turns and a core diameter of 200mm was tightly wound using rectangular copper wire of dimensions 7.5 mm x 1.45 mm. An XYZ coordinate system was set up around the coil so that it was concentric about the z-axis. Inside this multi-turned coil the magnetostatic field was measured along several axial contours. These results were compared to field predictions calculated by the algorithm for a coil of similar dimensions.

Results.

Figs. 6.7 a and 6.7b show a comparison between measured and calculated field intensities inside the coil. An excellent correlation is evident from the results.

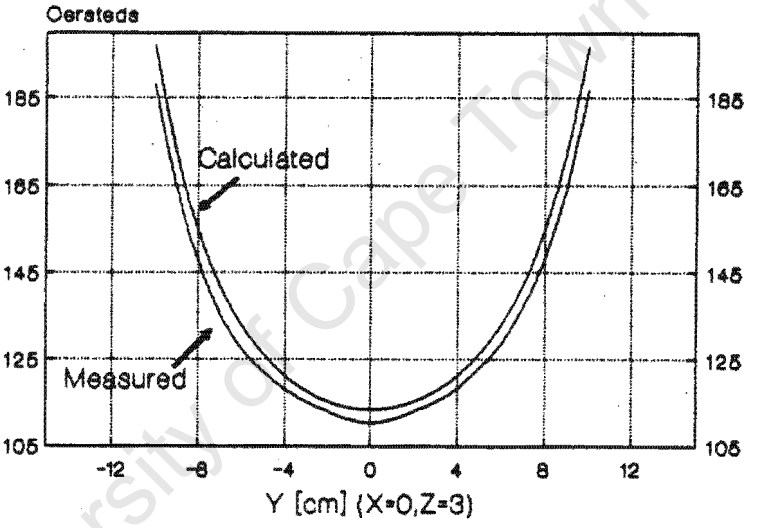

Figure 6.7a Measured versus Calculated magnetostatic field along the y axis contour where x = 0 and z = 3 cm. Coil turns = 14 x 8, wire dimensions = 7.5 x 1.45mm, I = 22 amps, coil diameter = 200mm.

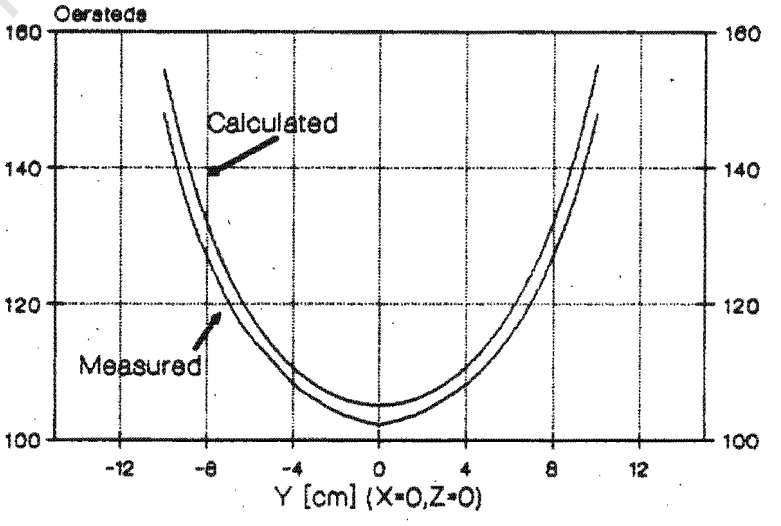

Figure 6.7b Measured versus Calculated magnetostatic field along the y axis contour where x = 0 and z = 0 cm. Coil turns = 14 x 8, wire dimensions = 7.5 x 1.45mm, I = 22 amps, coil diameter = 200mm.

C]

A coil having 10 x 10 turns and a core diameter of 40 mm was wound using rectangular copper wire having similar dimensions to B. The total length of conductor needed for this coil was +- 28 meters.A pulsed magnetic field was generated for this coil by discharging a 996 +- 10 μF capacitor bank, charged to a voltage of 1000 volts into the coil. Coil inductance and resistance measured at Dc was 197 μH and 45 milliOhms respectively. The field was measured at several typical points inside the coil.

Results:

The changed AC impedance that includes "skin-effect" for a coil with the above specifications, is approximated by Eqn 5.1 with $\alpha_1 = 36 \times 2\pi$, $\alpha_2 = 6025 \times 2\pi$ π, $\beta_1 = 6000 \times 2\pi$. The magnitude of components for the coil's new equivalent circuit are L1 = 199 μH, R1 = 45 mOhms, L2 = 47.8 mH, R2 = 1082.3 Ohms. With these components values of a,b and c of Eqn. 5.4 are solved numerically to a = 113.7, b = 2248.5, c = 37842.5. The current pulse flowing through the coil defined by Eqns 5.5 and 5.6 is shown in Fig. 6.8, where t_{peak} = +-0.6743 msec, I_{peak1} = 2071.3 and I_{peak2} = 0.084.

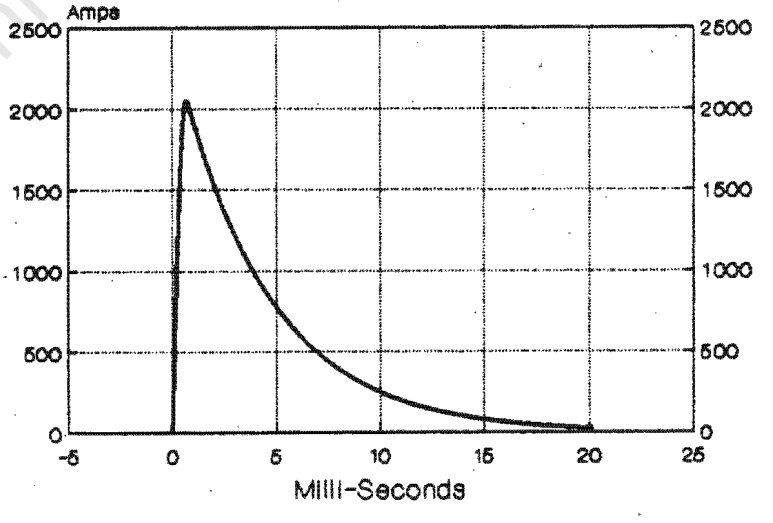

Figure 6.8 Magnetising current pulse for a magnetiser where the coil is approximated by an equivalent circuit to account for eddy current losses.

If the time period of this pulse is assumed to be 128 x tpeak the discrete frequency spectrum of this pulse is shown by Fig. 6.9.

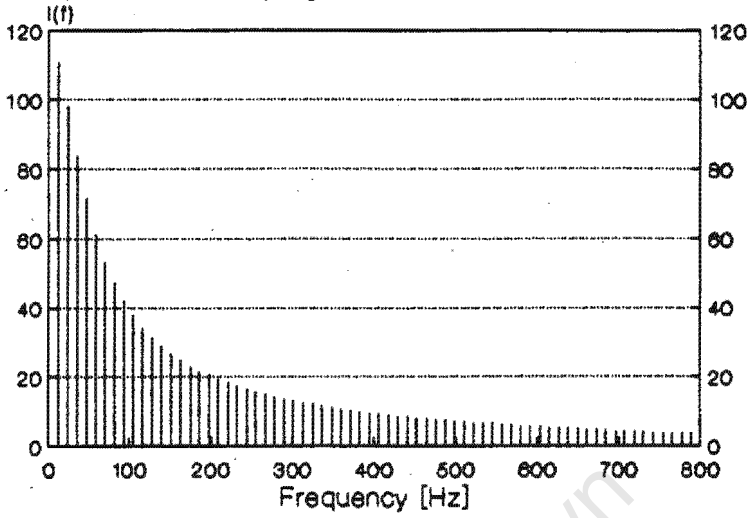

Figure 6.9 Discrete frequency spectrum of the magnetising current pulse shown by Fig 6.8 which is assumed to be periodic with a time duration of 20 x t_{peak}

The eddy current algorithm described in chapter 4 must be applied for each frequency component when solving the field in Eqns 5.9 - 5.11. Figures 6.10a and 6.10b show measured and calculated time dependent field values at typical points inside the coil. An excellent agreement is seen in the figures. Of importance is the large-scale difference in magnitudes of the field at these two points demonstrating the non-uniformity and complexity of the field.

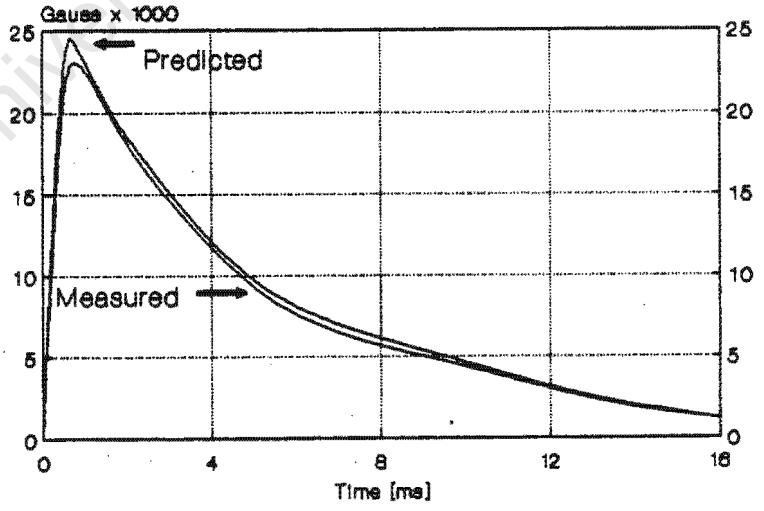

Figure 6.10a Measured and Calculated (with eddy losses) pulsed magnetic field at the point (0,0,40) inside the 10 x 10 turned coil of C

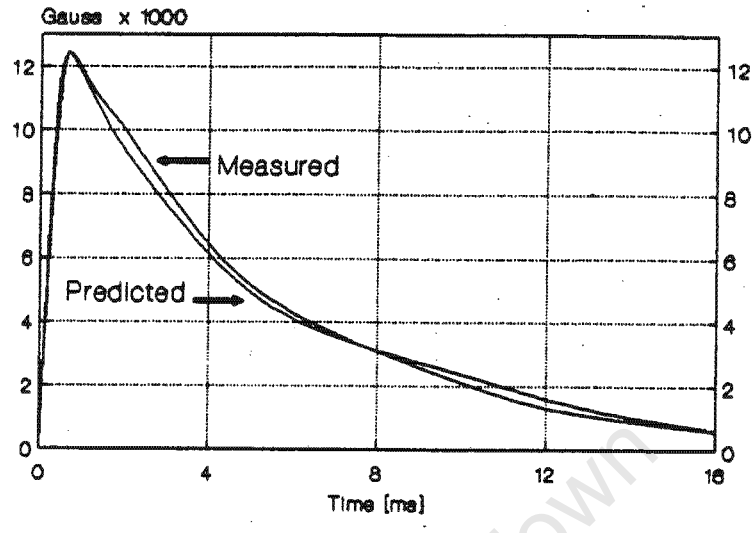

Figure 6.10b Measured and Calculated (with eddy losses) pulsed magnetic field at the point (10,0,0) inside the 10 x 10 turned coil of C

To determine the effect of eddy current losses, the field was calculated at identical points using the current density approximation Eqn 5.13. Table 4, lists a comparison of the field at several time instances. From Table 4 an average loss of +- 2 % occurs for the field due to the "skin-effect".

Time	Magnetic Field H(rp) [A/m]			
msec	(0,0,45) Eddy Losses (10,0,0)			
	yes	no	yes	no
0.135	5923.58	5964.53	3000.71	3021.46
0.270	11412.70	11495.38	5781.33	5823.22
0.405	16208.74	16324.82	8210.87	8269.67
0.539	20088.09	20226.33	10176.03	10246.06
0.674	22877.75	23025.06	11589.19	11663.82
0.809	24463.01	24605.44	12392.24	12464.39
0.944	24827.72	24957.57	12576.99	12642.77
1.079	22043.26	22139.37	11166.46	11215.15

TABLE4

D].

The pulsed magnetic field was calculated at a point inside a 10 - turned coil of diameter 40mm made from wire of dimensions 10mm x 10mm (ie. larger cross-sectional conductor area than the coil in C). Table 5 lists a comparison of the field calculated at several time instances with the field calculated using the approximation current density Eqn 5.13, where eddy current losses are neglected.

Results:

From Table 5 a difference of +- 3 % is observed between the results.

Time [msec]	Pulsed Magnetic Field [A/m] (with Eddy)	(without eddy)	Difference %
0.172	12697	12940	1.8
0.3425	17928	18277	1.9
0.5137	17663	18152	2.7
0.6850	17467	18027	3.1
0.8562	17309	17904	3.3
1.0275	17171	17781	3.4
1.1981	17046	17660	3.5

TABLE5

REFERENCES

[15] S.Babic, Z. Andjelic, B. Krystajic, S. Salon, "Analytical Calculation of the 3D Magnetostatic Field of a Torroidal conductor with Rectangular Cross Section", IEEE Trans on Magn, Vol Mag-24, No 6, Nov 1988, Pg 3163 - 3164.

[16] William R. Smythe, Static and Dynamic Electricity, New York and London, McGraw-Hill Book company Inc, 1939, 1st Edition Pg. 266.

[17] Smythe, Pg.273, see [16].

7 CONCLUSIONS.

A mathematical algorithm has been formulated that can be used to design a magnetising coil made from copper wire of rectangular cross-sectional area. In view of the results from chapter 6 , the following conclusions may be drawn:

7.1. The magnetic field generated in a coil is dependent upon the conductors physical dimensions and on how the coil is wound. The algorithm presented in this report accurately describes this dependency by using a model helical turn to simulate the windings of a physical wire-wound coil. (sections 6.1A, 6.1B 6.2A and 6.2B)

7.2. The Algorithm is able to approximate the pulsed magnetising field very well inside coils of different configurations.(section 6.2 C).

7.3. Eddy current effects may have a minimal effect on the pulsed magnetising field if the bandwidth is within 2Khz (eg the magnetiser in section 6.2 C).

7.4. Total eddy current losses are dependent on the magnetiser set-up. Eg.Decreasing the magnetising pulse time duration will increase the pulses bandwidth and thus increase losses. Also using a coil conductor with larger cross-sectional area causes greater losses (section 6.2 D).

7.5. The algorithm can be used to help design magnetising coils that will generate field intensities of sufficient strength to saturate some ferromagnetic material for a given magnetiser set-up.

8. PRACTICAL MAGNETISER WITH APPLICATIONS

Photographs in Figs 8.1 - 8.7 show the prototype magnetiser set-up used for his project (see specifications in Table 6). All measurements to confirm the accuracy of the Field algorithm was performed with this equipment. Noteworthy, but not mentioned in this report because of its irrelevance to the topic, is the "self-constructed" vacuum switch. This switch was constructed to find a suitable low-cost option for switching high voltages "cleanly", and exploited the characteristic voltage breakdown properties of a vacuum. Tests performed with this switch were very encouraging and as a direct result the company G.E.C. donated a vacuum interupter to aid the project.

PROTYPE MAGNETISER DATA	
Charging components	
Voltage source	4000 volts
Capacitor Bank	996 microFarads 4000 volts
Coil Data	
Ldc	197 microHeries
Rdc	45 milli Ohms
No turns	10 x 10
Pitch of turn	8.5mm
Conductor size	1.45 mm x 7.5 mm
Radius core	19 mm
Switches	
Voltage < 1200 volts	- Thyristor
Voltage > 1200 volts	- Vacuum switch

TABLE 6